applied sciences

MDPI

Article

Are Quantitative Errors Reduced with Time-of-Flight Reconstruction When Using Imperfect MR-Based Attenuation Maps for ^{18}F-FDG PET/MR Neuroimaging?

Jani Lindén [1,2,*,†], Jarmo Teuho [1,3,4,†], Riku Klén [1,3] and Mika Teräs [4,5]

1 Turku PET Centre, University of Turku, 20520 Turku, Finland; jarmo.teuho@tyks.fi (J.T.); riku.klen@utu.fi (R.K.)
2 Department of Mathematics and Statistics, University of Turku, 20500 Turku, Finland
3 Turku PET Centre, Turku University Hospital, 20520 Turku, Finland
4 Department of Medical Physics, Turku University Hospital, 20521 Turku, Finland; mika.teras@tyks.fi
5 Institute of Biomedicine, University of Turku, 20520 Turku, Finland
* Correspondence: jjlind@utu.fi
† These authors contributed equally to this work.

Abstract: We studied whether TOF reduces error propagation from attenuation correction to PET image reconstruction in PET/MR neuroimaging, by using imperfect attenuation maps in a clinical PET/MR system with 525 ps timing resolution. Ten subjects who had undergone ^{18}F-FDG PET neuroimaging were included. Attenuation maps using a single value (0.100 cm^{-1}) with and without air, and a 3-class attenuation map with soft tissue (0.096 cm^{-1}), air and bone (0.151 cm^{-1}) were used. CT-based attenuation correction was used as a reference. Volume-of-interest (VOI) analysis was conducted. Mean bias and standard deviation across the brain was studied. Regional correlations and concordance were evaluated. Statistical testing was conducted. Average bias and standard deviation were slightly reduced in the majority (23–26 out of 35) of the VOI with TOF. Bias was reduced near the cortex, nasal sinuses, and in the mid-brain with TOF. Bland–Altman and regression analysis showed small improvements with TOF. However, the overall effect of TOF to quantitative accuracy was small (3% at maximum) and significant only for two attenuation maps out of three at 525 ps timing resolution. In conclusion, TOF might reduce the quantitative errors due to attenuation correction in PET/MR neuroimaging, but this effect needs to be further investigated on systems with better timing resolution.

Keywords: PET; TOF reconstruction; attenuation correction

Citation: Lindén, J.; Teuho, J.; Klén, R.; Teräs, M. Are Quantitative Errors Reduced with Time-of-Flight Reconstruction When Using Imperfect MR-Based Attenuation Maps for ^{18}F-FDG PET/MR Neuroimaging? *Appl. Sci.* **2022**, *12*, 4605. https://doi.org/10.3390/app12094605

Academic Editors: Aristotelis Chatziioannou and Marco Giannelli

Received: 9 February 2022
Accepted: 20 April 2022
Published: 3 May 2022

1. Introduction

Since the introduction of the first time-of-flight (TOF)-capable positron emission tomography (PET) systems, several advances have been made in terms of PET detector technology and achieving even higher timing resolutions. Recent developments in positron emission tomography/magnetic resonance (PET/MR) instrumentation have paved the way to TOF-capable PET/MR systems by using digital PET detectors [1,2]. From the PET/MR systems available in the clinical market, the GE Signa PET/MR, the United Imaging uPMR 790 HD TOF PET/MR, and the Philips Ingenuity TF PET/MR are capable of TOF imaging [1–3]. The timing resolution of the systems are reported as 390 ps for the Signa, 480 ps for uPMR 790, and 525 ps for the Ingenuity TF [1]. Recently, an even higher timing resolution has been reported with a clinical PET/CT system, up to 210 ps [4]. These developments could result in several advantages especially in PET/MR imaging which are highlighted below.

The inclusion of TOF in combined PET/MR systems can be considered beneficial due to a multitude of reasons. The visual quality of PET images can be improved by the higher

contrast and signal-to-noise ratio (SNR) which TOF offers [5]. The use of TOF also offers additional advantages in robustness. The TOF reconstruction converges faster, especially with higher time resolution, and is more resilient to errors in normalization, scatter, and attenuation correction, due to the addition of additional constraints and reduced cross-dependencies between image voxels [6–8]. By including TOF information, only the image voxels along the segments of the line of response defined by the TOF resolution can be updated at each iteration, instead of all the voxels along the line of response [7]. The error propagation in TOF imaging can be considered to be proportional to TOF timing resolution, whereas in non-TOF reconstruction the errors are proportional to object size [9]. Therefore, using TOF in combined PET/MR has potential in producing PET images with higher visual and quantitative accuracy due to a reduced sensitivity to errors, especially when inconsistencies in attenuation correction occur.

Previous studies have also highlighted several visual and quantitative benefits when applying TOF reconstruction. It has been shown that TOF decreases quantitative and visual errors due to MR-based attenuation correction (MRAC) in whole-body PET imaging, such as in cases of metal artifacts [10], susceptibility artifacts [11], defective PET detectors [12], a variety of PET artifacts [13] including implants [14], and MRAC in general [7]. Studies have shown that TOF reduces PET quantification errors when using MRAC, reducing the error propagation from attenuation maps to PET images [15]. Future systems with increased TOF timing resolution could enable the reduction of artifacts and quantification to an even larger degree [7]. Thus, applying TOF in combination of MRAC could be considered highly beneficial. However, these studies have been mainly performed and shown benefits for whole-body PET only.

While these benefits are evident for whole-body imaging, the effect of TOF should be investigated for other body regions as well. Recently, it was shown that increasing the TOF resolution might increase error propagation to neighboring regions, and the effect of this error propagation can no longer be considered local [16]. In a simulation study performed in the lung region with different timing resolutions, it was shown that the errors in TOF-reconstructed regions increased or decreased in accordance with the non-TOF reconstruction [16]. This factor has important implications for neuroimaging, where it is desirable not just to reduce the global bias but to minimize regional variation as well. Thus, the error propagation in TOF reconstruction using imperfect attenuation maps should be further investigated for brain PET/MR imaging.

Whereas MRAC in neuroimaging has been an area of extensive research since the introduction of clinical PET/MR systems [17,18], the benefits of TOF have not been thoroughly investigated for neurological PET/MR imaging. In this regard, we set out to investigate how TOF reconstruction affects the quantitative accuracy of PET when using imperfect attenuation maps for MRAC and evaluated its effect on regional bias in PET both globally and locally. Our goal was to investigate whether using TOF is beneficial in reducing the quantitative errors due to MRAC in the gray matter with a clinical 525 ps timing resolution PET/MR. We set out to investigate if the inclusion of TOF would result in error reduction and better concordance to CTAC reconstructed PET both globally and locally when using MR-based attenuation maps of varying accuracy.

2. Materials and Methods

2.1. Patient Data

A cohort of clinical subjects were used in this retrospective study. The subjects had undergone a PET/MR and a PET/CT examination on the Philips Ingenuity TF PET/MR and the GEHC Discovery 690 PET/CT. The performance evaluation of both systems can be found in their respective articles [1,19].

The cohort consisted of ten subjects (three males, seven females) suspected of memory disorders. The subjects had undergone both PET/CT and PET/MR during the same imaging session (seven subjects) or had PET/CT and PET/MR performed on separate days (9 d; 6 mo. 19 d; and 7 mo. 3 d apart). The mean and standard deviation of subject age,

weight, and injected dose of ^{18}F-FDG were: 53 ± 14 years, 73 ± 19 kg, and 277 ± 47 MBq. The mean ± standard deviations of the scan start times were 80 ± 20 min after the injection for the group which had undergone imaging during subsequent sessions.

All PET/CT and PET/MR acquisitions were performed using the standard protocol for neurological imaging at our center. The PET acquisition on the PET/MR was performed in list-mode with the acquisition time of 15 min over one bed position, with a transaxial acquisition field of view of 256 mm × 256 mm.

The study was conducted as a retrospective registry study at Turku PET Centre (study number: T7/2021). The need to acquire an active informed consent from the individuals included in the study was waived and the study protocol was approved by Turku University Hospital Research Board and the legislative team. The requirements for ethical review in Finland are stipulated primarily in the Medical Research Act (488/1999, as amended) and the Act of the Medical Use of Human Organs, Tissues and Cells (101/2001 as amended). Ethical review is statutorily required for interventional medical research and some circumstances for studies on human organs, tissues, or cells. According to Finnish legislation, no ethical assessment or approval by an independent review board is mandatory for registry studies. The study was conducted in accordance with the Declaration of Helsinki.

2.2. CTAC Data

The CT-based attenuation correction (CTAC) from the PET/CT acquisition was used to create the reference attenuation map for the method comparison. All CTAC data was collected with a low-dose CT acquisition, using a tube voltage of 120 kV, which was transformed to linear attenuation coefficients by the bi-linear transformation described by Burger et al. [20] and processed similarly, to what has been reported in [21] for the Ingenuity TF PET/MR system. CTAC was completed with soft tissue from the MRAC if the field of view (FOV) of the CTAC was smaller than MRAC.

2.3. MRAC Data

The MR data for attenuation correction was collected with a 3D T1-weighted fast field echo sequence with echo time of 2.16 ms, repetition time of 4.18 ms and a flip angle of 10 degrees. The geometry correction on the MRI system is applied with the option value set as "default". In total, three MR-based attenuation maps were created: (a) soft tissue (0.096 cm^{-1}), bone (0.151 cm^{-1}), and air (3-class model), (b) soft tissue with higher mu-value of 0.100 cm^{-1} and air cavities (2-class model), and (c) a higher mu-value of 0.100 cm^{-1} for all soft tissue and ignoring all air cavities inside the head (2-class model without air).

All the MR-based attenuation maps, including the 3-class model were created from the T1-weighted images with an SPM8-based method described in an earlier study [22]. The 2-class model was created by assigning the same attenuation coefficient for both the bone and soft tissue. Finally, in the 2-class model without air, the air cavities inside the head were ignored in the segmentation pipeline. The less accurate attenuation maps cannot be expected to perform as well as the 3-class model and thus the focus of the study is to evaluate the effects of TOF when attenuation maps are inaccurate rather than compare the results of different attenuation maps to each other.

2.4. Importing CTAC and MRAC to PET Reconstruction

Before PET image reconstruction, both the CTAC and MRAC were co-registered to non-attenuation corrected (NAC)-PET images to ensure the best possible registration between the attenuation map and PET data. The registration was performed using normalized mutual information as implemented in SPM8. Afterwards, all CTAC and MRAC images were visually inspected against PET data to confirm the registration accuracy. An example of the different attenuation maps is shown in Figure 1. The MR hardware components including the patient table and the head coil were included in the final attenuation map, inserted automatically by the PET reconstruction software.

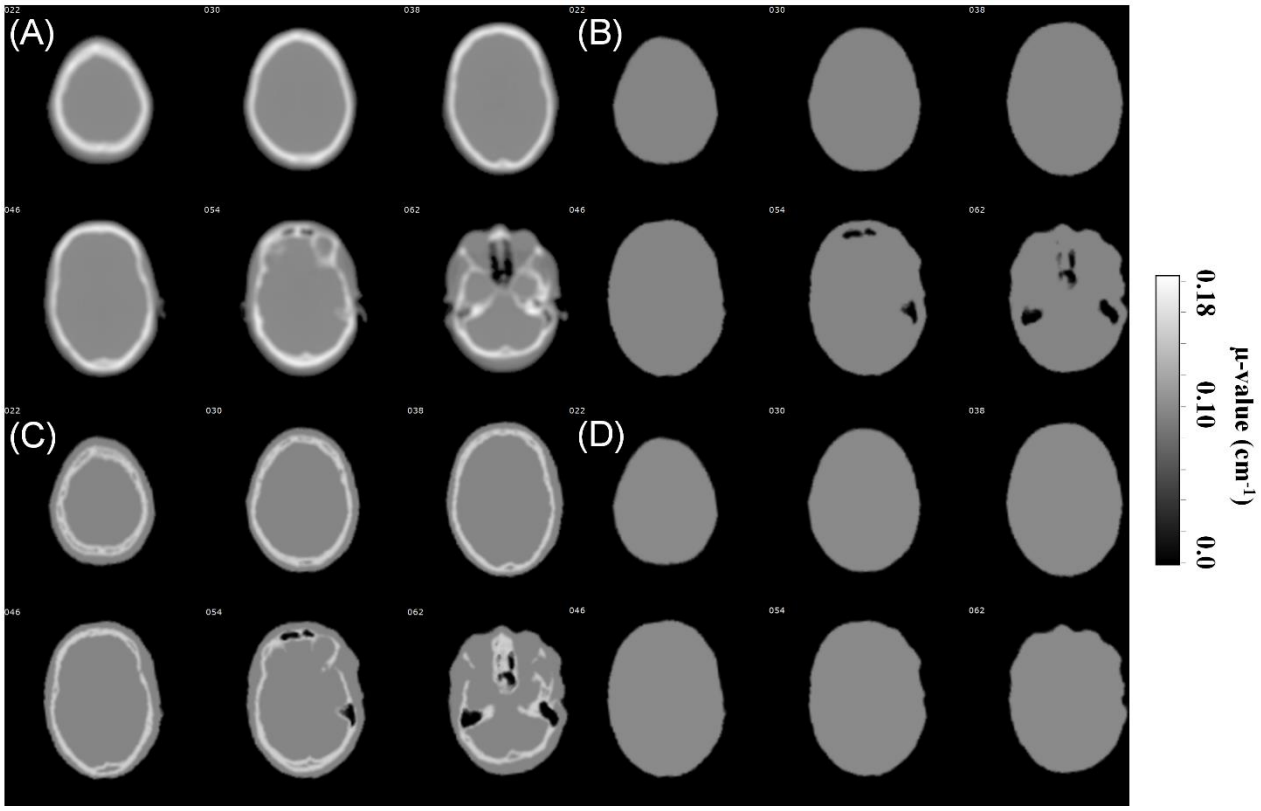

Figure 1. Different attenuation maps used in the PET image reconstruction, with (**A**) CTAC, (**B**) 2−class MRAC with attenuation coefficient of 0.100 cm^{-1} for all tissues, (**C**) 3−class MRAC, (**D**) 2−class MRAC with attenuation coefficient of 0.100 cm^{-1} and ignoring air cavities.

2.5. PET Reconstruction Protocol

All PET reconstructions were performed using a non-TOF line-of-response row expectation maximum algorithm (LOR-RAMLA) and a TOF ordered subset expectation maximum (TOF-OSEM, vendor name: BLOB-OSEM-TF) algorithm. The image matrix size for all reconstructions was 128 × 128 × 90 pixels with 2 mm isotropic voxel resolution. We used the default reconstruction parameters for LOR-RAMLA and BLOB-OSEM-TF, which were alpha = 6.3716, radius = 2.8, blob increment = 2.0375, and relaxation parameter = 0.035 for LOR-RAMLA. For TOF reconstruction, the reconstruction parameters used were alpha = 4.1338, radius = 2.3, blob increment = 2.0375, and relaxation parameter = 1.00. Reconstructions were performed with 2 iterations and 33 subsets with LOR-RAMLA and 3 iterations and 33 subsets with TOF-OSEM.

2.6. PET Image Analysis

PET image quality was inspected visually and quantitatively. Mean PET images across all patients corresponding each MRAC method were created using non-TOF and TOF reconstruction. For creation of mean PET images, all PET images of each subject were transformed from individual space to Montreal Neurological Institute (MNI) space and were spatially normalized using the normalization tools of SPM8.

A quantitative analysis was performed using 35 volumes of interest (VOI) in the cortical regions from the automatic anatomical labelling atlas (AAL). The absolute difference to *CTAC* reconstructed *PET* was calculated for each VOI with each of the *MRAC* method, using Equation (1):

$$\Delta\% = \frac{PET_{MRAC} - PET_{CTAC}}{PET_{CTAC}} \times 100\%. \quad (1)$$

A statistical comparison was also performed by linear regression and Bland–Altman analysis between *CTAC* reconstructed PET VOI values and *MRAC* reconstructed PET VOI values in both TOF and non-TOF reconstructed PET. Linear regression coefficients are tested for statistical significance with F-test, and their confidence intervals were calculated as Wald intervals [23].

The differences in average VOI biases between non-TOF and TOF reconstructions were tested for statistical significance. First, the normality of the distributions was assessed with Shapiro–Wilk's test at 95% significance level. One distribution, the 3-class model with TOF reconstruction, did not pass the Shapiro–Wilk test of normality. Thus, the Wilcoxon's signed rank test was used to investigate whether inclusion of TOF had a statistically significant difference on the average VOI bias distributions.

Pairwise comparisons were done with Wilcoxon's signed rank test with 95% significance level and a p-value < 0.05 denoting statistical significance. The Benjamini–Hochberg method [24] with 5% false discovery rate (FDR) to account for multiple comparisons was used. In the Benjamini–Hochberg method, the comparisons are sorted in ascending order and then given a rank $\{1, \ldots, n\}$ based on their position. Then, all comparisons are considered statistically significant that have a rank smaller or equal than the largest rank where $p < \frac{r}{n} \times FDR$ where p is the p-value of a comparison and r is the rank of the comparison, and n is the total number of comparisons.

To inspect the differences between each of the method locally, bias atlas images were created according to [25] from each method across all subjects. Mean bias and standard deviation of bias across the whole subject group with each of the MRAC method were then calculated and visualized.

3. Results

Figure 2 shows the relative distribution of bias across all the 35 regions of the brain. The distribution of bias is smaller in the TOF reconstructed images and majority of the subjects (8/10 in 3-class and 7/10 in 2-class MRAC) show a reduced bias across all the attenuation maps when TOF reconstruction is applied. Overall, the median differences are small (within 1%) between TOF and non-TOF reconstructions. The VOI averages can be seen in Table A1, where TOF showed a maximum error reduction of 3% in the region of the vermis. The reduction of bias was smaller when the accuracy of the attenuation map increased, meaning the PET reconstruction using an attenuation map with the least accuracy gained the most benefit from TOF.

Figure 3 shows the regression plots with all attenuation maps with TOF and non-TOF reconstruction. The TOF reconstructions shows only minor changes in correlation to CTAC reconstructed PET across all MRAC methods. Distribution of data points is narrower with TOF reconstruction.

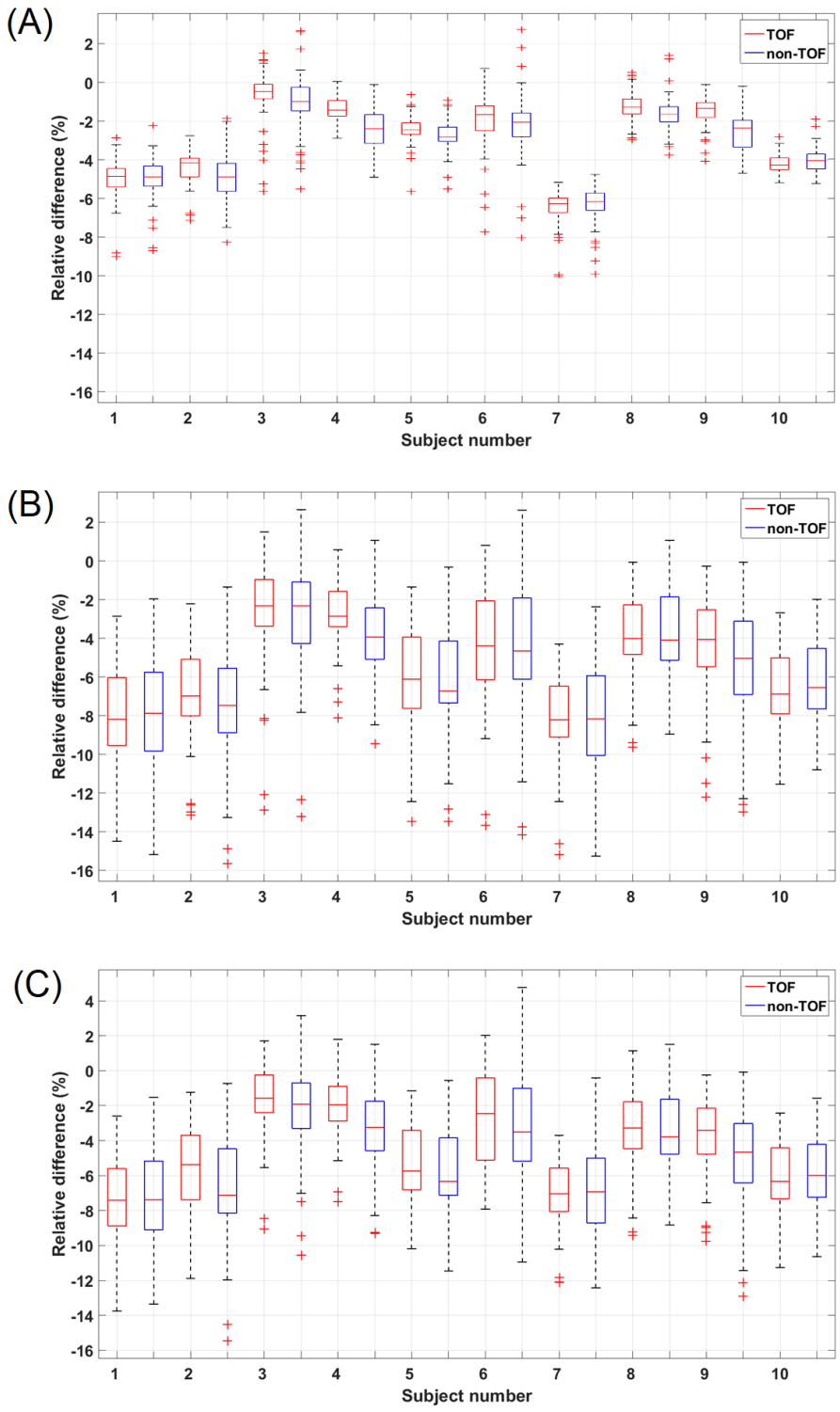

Figure 2. Box and whisker plots of the relative difference to CTAC reconstructed PET when using TOF and non−TOF reconstructed images. (**A**) 3−class MRAC, (**B**) 2−class MRAC, (**C**) 2−class MRAC without air cavities. The box plots show the results of each patient using the set of 35 VOIs' mean bias as data. For each subject, the red TOF box plot is presented first, followed by blue non-TOF box plot immediately to its right. Outlier values are denoted with red '+' symbol. A value beyond the maximum whisker length of 1.5 times the quartile range is considered an outlier.

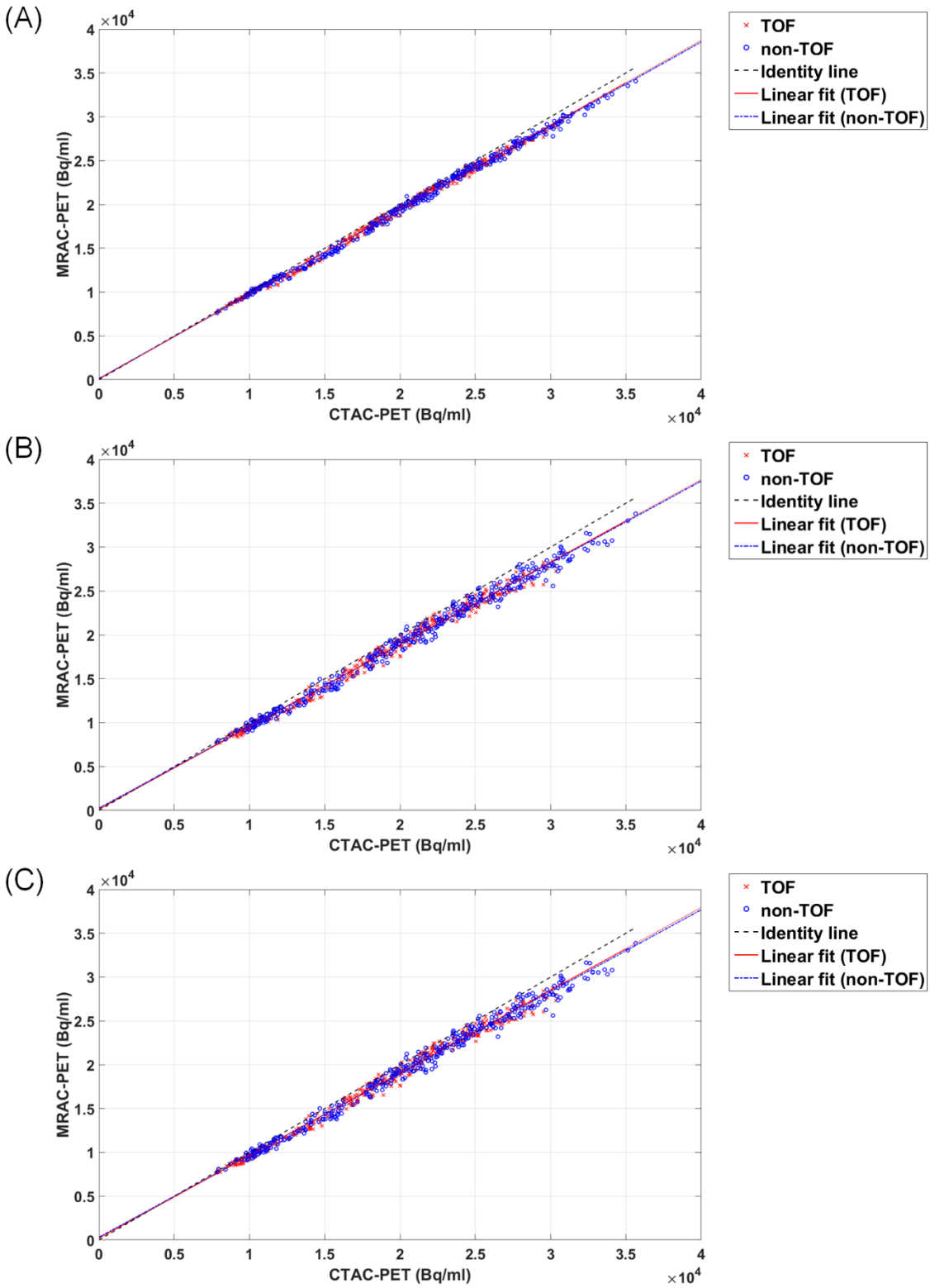

Figure 3. Regression plots of non-TOF (marked as blue 'o' symbol) and TOF (marked as red '×' symbol) reconstructed activity values with different MRAC methods versus CTAC reconstructed PET. (**A**) 3−class MRAC, (**B**) 2−class MRAC, (**C**) 2−class MRAC without air cavities.

Table 1 contains the fitting coefficients and R^2 values from the correlation analysis. The R^2 values are similar with 3-class MRAC with and without TOF. The TOF reconstruction with 2-class MRAC shows an improved R^2. All correlations are statistically significant,

and the 95% confidence intervals are close to each other between non-TOF and TOF reconstructions. The regression coefficients all improve, as coefficients *a* approach 1 and coefficients *b* approach 0 when TOF reconstruction is used. However, the confidence intervals for coefficient *a* overlap between TOF and non-TOF reconstructions, albeit very narrowly, meaning that the detected differences are not statistically significant. Two out of three coefficients *b* with TOF reconstruction are not significantly different from zero, while all non-TOF coefficients *b* are. This indicates improvement, even if all confidence intervals for coefficients *b* include their counterpart estimate as well, denoting the differences are not statistically significant.

Table 1. Fitting coefficients *a* (slope) and *b* (intersect) for linear regression and R^2 values from the correlation analysis. Confidence intervals (CI) and *p*-values for regression and correlation coefficients are also presented. Coefficient *b* does not differ significantly from zero for 3-class MRAC TOF and 2-class MRAC TOF. Coefficient *a* and R^2 value are statistically significant for all methods.

Method		*a*	*b*	*a* *p*-Value	*b* *p*-Value	*a* 95% CI	*b* 95% CI	R^2	R *p*-Value	R 95% CI
3-class MRAC	TOF	0.966	89.1	<0.001	0.142	[0.9595, 0.9717]	[−30.06, 208.32]	0.996	<0.001	[0.9978, 0.9986]
	non-TOF	0.960	134	<0.001	0.030	[0.9544, 0.9656]	[12.77, 254.80]	0.997	<0.001	[0.9981, 0.9988]
2-class MRAC	TOF	0.938	152	<0.001	0.115	[0.9286, 0.9479]	[−37.25, 341.09]	0.991	<0.001	[0.9942, 0.9962]
	non-TOF	0.932	256	<0.001	0.022	[0.9216, 0.9418]	[37.25, 474.32]	0.990	<0.001	[0.9935, 0.9957]
2-class MRAC (no air cavities)	TOF	0.943	211	<0.001	0.027	[0.9336, 0.9527]	[23.59, 398.48]	0.991	<0.001	[0.9943, 0.9963]
	non-TOF	0.934	320	<0.001	0.003	[0.9241, 0.9439]	[104.95, 534.89]	0.990	<0.001	[0.9938, 0.9959]

Figure 4 shows the Bland–Altman plots with all the attenuation maps with TOF and non-TOF reconstruction. Limits of agreement and the mean bias are slightly smaller with the TOF reconstruction across all MRAC methods.

The results from statistical testing are given in Table 2. For the 2-class MRAC without air and the 3-class MRAC, the changes were statistically significant at 95% significance level with $p = 0.018$ and $p < 0.001$, respectively. Using the Benjamini–Hochberg method with FDR set to 5%, the null hypothesis of equal medians can be rejected for both 2-class MRAC without air and the 3-class MRAC, meaning that these two MRAC methods gained significant improvements when applying TOF reconstruction even after correction for multiple comparisons.

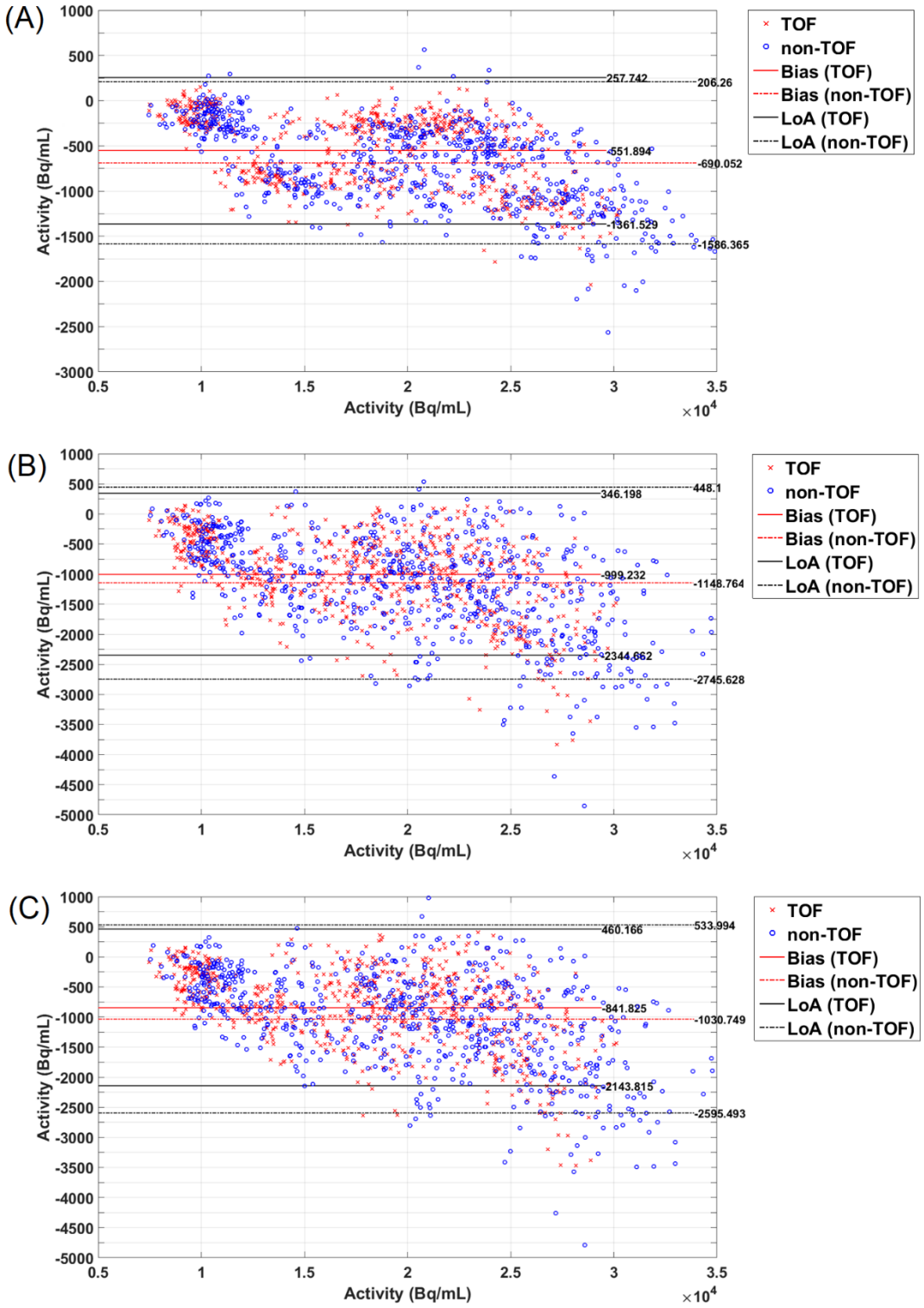

Figure 4. Bland–Altman plots of non-TOF (marked as blue 'o' symbol, and dashed lines) and TOF (marked as red '×' symbol and solid lines) reconstructed activity values with different MRAC methods versus CTAC reconstructed PET. (**A**) 3−class MRAC, (**B**) 2−class MRAC, (**C**) 2−class MRAC without air cavities. The horizontal lines correspond to mean bias and limits of agreement (LoA).

Table 2. Results of the Wilcoxon's signed rank test. Median difference denotes the median of average VOI errors in TOF vs. non-TOF reconstructions. The significance thresholds of the Benjamini–Hochberg method are given, and statistically significant *p*-values are denoted with *.

Method	Median Difference (TOF vs. Non-TOF)	*p*-Value (Two-Tailed)	Benjamini–Hochberg Significance Threshold
3-class MRAC	−2.9% vs. −3.3%	<0.001 *	0.0166
2-class MRAC	−5.7% vs. −5.9%	0.224	0.0500
2-class MRAC (no air cavities)	−4.7% vs. −5.4%	0.018 *	0.0333

Figure 5 shows the mean PET images with all the methods. Small local improvements can be seen with the TOF reconstruction.

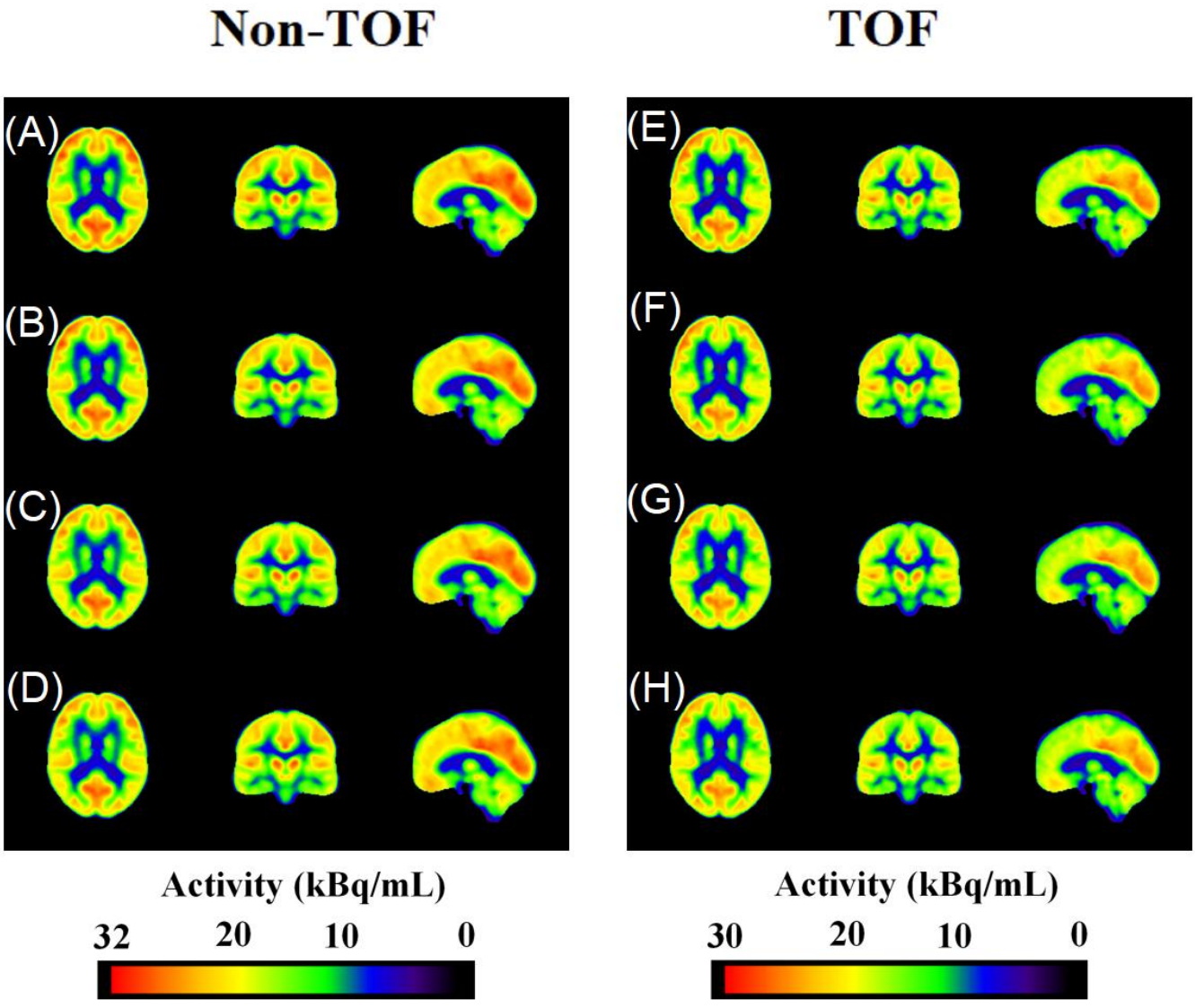

Figure 5. Mean PET images reconstructed with different attenuation maps compared between non-TOF and TOF reconstruction. A small benefit when using TOF reconstruction can be seen, although the visual differences are small. (**A**) CTAC, (**B**) 3−class MRAC, (**C**) 2−class MRAC, (**D**) 2−class MRAC without air cavities using non-TOF reconstruction. (**E**) CTAC, (**F**) 3−class MRAC, (**G**) 2−class MRAC, (**H**) 2−class MRAC without air cavities using TOF reconstruction.

Figure 6 shows the bias atlas images with all the methods. Local improvements can be seen with the TOF reconstruction especially in the sinus region. The bias is generally reduced in the cortical regions and across the brain with TOF.

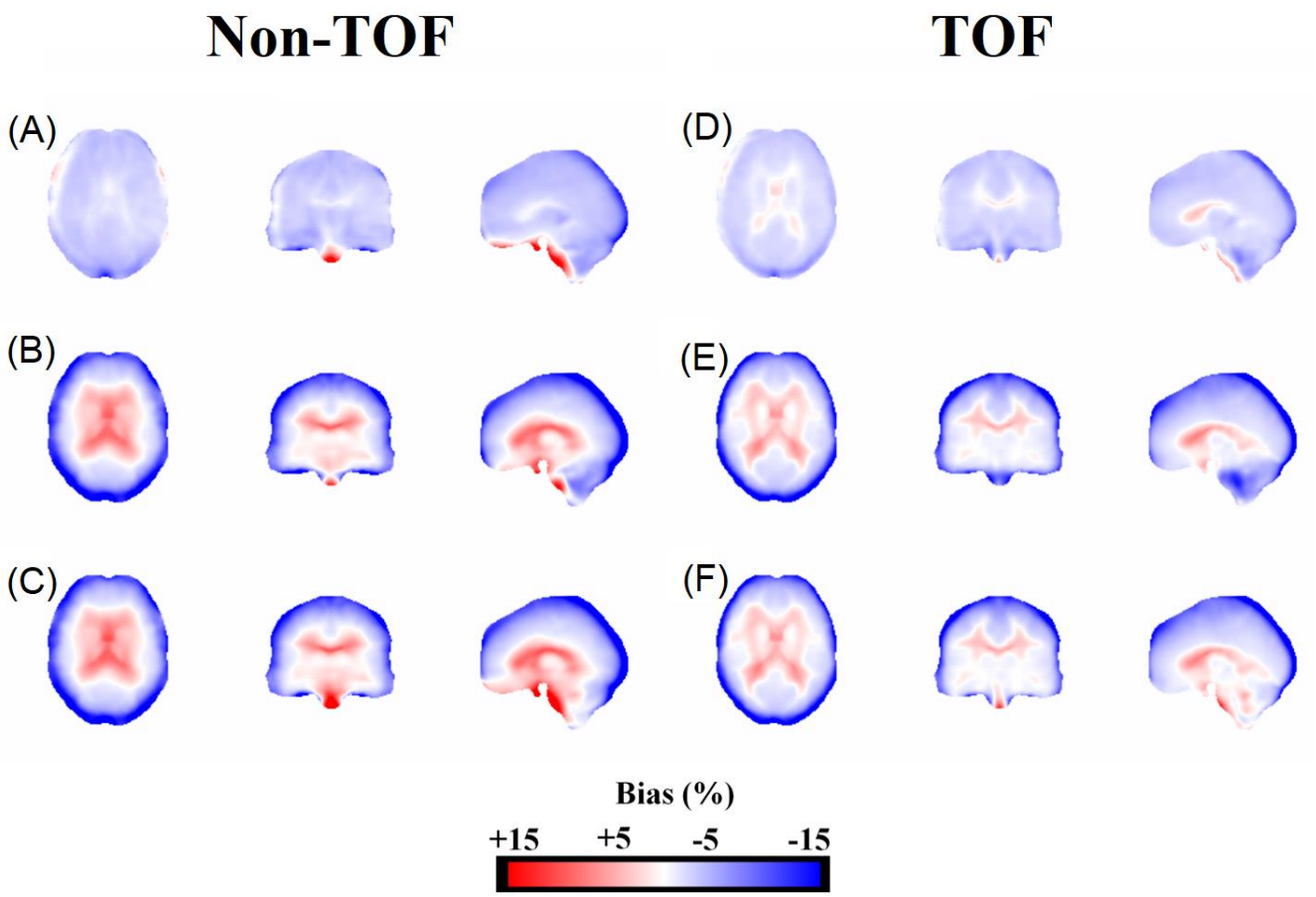

Figure 6. Mean bias atlas images from non−TOF and TOF reconstructed PET. A clear reduction of bias is seen in the TOF reconstructed images across the brain compared to non−TOF reconstructed PET. (**A**) 3−class MRAC, (**B**) 2−class MRAC, (**C**) 2−class MRAC without air cavities using non−TOF reconstruction. (**D**) 3−class MRAC, (**E**) 2−class MRAC, (**F**) 2−class MRAC without air cavities using TOF reconstruction.

Figure 7 shows the bias standard deviation images with all the methods. Small local improvements can be seen with the TOF reconstruction with a systematic reduction of standard deviation throughout the brain.

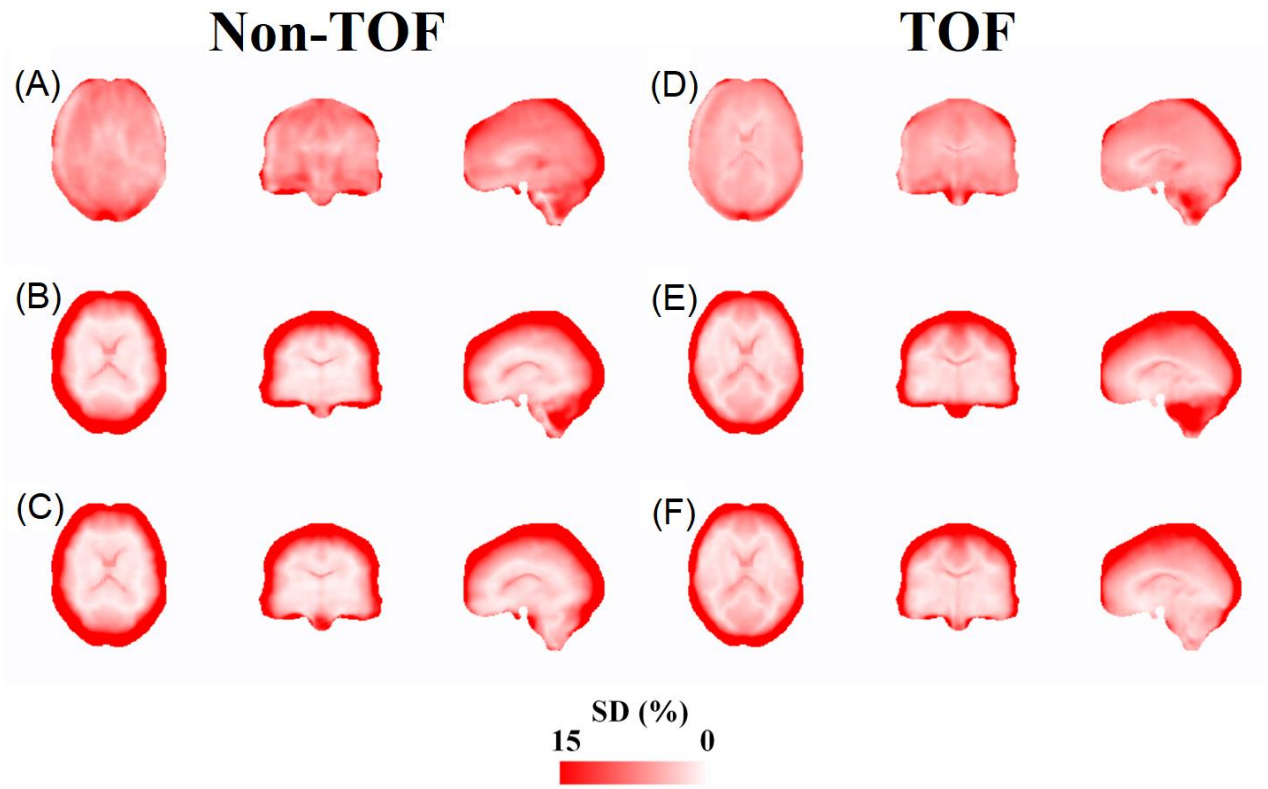

Figure 7. Bias standard deviation images with all the methods. Small local improvements can be seen with the TOF reconstruction with a systematic reduction of standard deviation throughout the brain. (**A**) 3−class MRAC, (**B**) 2−class MRAC, (**C**) 2−class MRAC without air cavities using non−TOF reconstruction. (**D**) 3−class MRAC, (**E**) 2−class MRAC, (**F**) 2−class MRAC without air cavities using TOF reconstruction.

4. Discussion

The effect of TOF imaging in reducing the errors due to imperfect MRAC in the head region was investigated. The results show that TOF reconstruction reduced the visual and quantitative errors in the head region of MRAC, although the overall effect was small. The effect was seen in the majority of the head regions independent of the accuracy of the attenuation map. The gains in quantitative accuracy were in part dependent on the anatomical location and the accuracy of the attenuation map, as TOF resulted in reduction of both over- and underestimations compared to the non-TOF reconstruction. Overall, a better concordance, although slight as well, to CTAC reconstructed PET was achieved when TOF information was applied in the image reconstruction and was statistically significant for two out of three MRAC methods.

In Figure 2, a reduction of bias can be seen when applying TOF with all the methods, although there is some variation by patient and the overall gain is small, within 1% of the methods. In some cases, the distribution of bias is also smaller with TOF, although the effect becomes less visible when the accuracy of the attenuation map decreases. Tables A1 and A2 show the mean and SD values for all brain regions separately. When using 3-class and 2-class (air included and excluded) attenuation maps, 26, 23, and 23 regions out of 35 showed lower absolute bias with TOF. Absolute bias increased in 9, 12, and 12 regions with TOF, respectively. The maximum gain due to TOF was 3% at maximum in one region and the gain reduced when the 3-class attenuation map was used (Table A1).

In Figure 3, the 2-class MRAC methods show that using TOF reduces the variance when compared to the non-TOF reconstruction. This can also be seen in Table 1, where R^2 values improve with TOF reconstruction for the 2-class methods; however, the differences were small, similarly to the VOI analysis. For the 3-class MRAC method, there are no

improvements in the R^2 value, as the more accurate attenuation map results in less variance to begin with. The TOF reconstruction also improves the linear regression fitting parameters by bringing slope a closer to the ideal value of 1 and lowering the intersect b towards the ideal value of zero for all methods. Two methods out of three showed non-significant differences with parameter b with TOF, indicating improvement. However, the changes between TOF and non-TOF reconstructions were not statistically significant for coefficients a and b as the 95% confidence intervals overlap (Table 1). These would indicate that despite TOF resulting in an improved correlation of MRAC reconstructed PET to CTAC reconstructed PET, the changes were altogether small and statistically non-significant.

The Bland–Altman graphs in Figure 4 show a similar reduction of error when TOF reconstruction is used. The non-TOF data points have wider distribution. The 2-class MRAC methods do not have clear differences between each other, but the 3-class MRAC has a tight error distribution in both non-TOF and TOF reconstruction, with TOF reconstruction having even less variance than the non-TOF reconstruction.

The statistical testing of the VOI differences from Table A1, presented in Table 2, confirmed that two out of the three MRAC methods (2-class method without air, and the 3-class method) showed statistically significant improvements in the average error when TOF reconstruction was used. The median differences in the average VOI errors were small in accordance with VOI analysis. The 2-class method showed non-significant differences between the TOF and non-TOF reconstruction after correction of multiple comparisons, indicating two methods out of three showed significant improvement when applying TOF.

In Figure 5, the TOF reconstruction shows lower maximum uptake than the non-TOF reconstruction. This is consistent with the results in Figure 3. This may indicate that image noise is suppressed more in the TOF reconstructed images, resulting in a lower maximum uptake. By using TOF, the local under- and overestimations in the PET data are also slightly reduced, bringing the TOF images closer to the CTAC reference (Figure 5), although this effect is small visually.

In Figures 6 and 7, the use of the TOF reconstruction resulted in the reduction of standard deviation and mean of the bias. This can be seen in the bias atlas images across all MRAC methods. These findings are similar to what has been reported previously in two whole-body studies [7,14]. For non-TOF reconstruction, there is overestimation near the sinus regions (Figure 6) for each of the MRAC methods but using TOF reconstruction corrects majority of it. Thus, TOF is beneficial in removing not just underestimation but overestimation due to attenuation correction errors.

Our results are in good agreement with previous studies. Khalife et al. compared several state-of-the art MRAC methods and concluded that the errors in the non-TOF reconstructions were significantly higher than with the TOF reconstructions [26], similarly to what was presented here. The paper also showed a lower median bias in TOF regardless of the MRAC method. However, looking closely at the results presented with no-bone CT and atlas-CT, the regional bias in the TOF reconstruction may not always be superior to the non-TOF reconstruction, indicating some regional variation remains in TOF similarly to our study. As the study was performed using a different PET/MR system with higher timing resolution (390 ps), this would indicate the effect exists also across systems and with different timing resolutions.

Finally, in this small proof-of-concept study, we have shown that TOF might be beneficial for neuroimaging PET studies performed on the PET/MR. Due to the low timing resolution (525 ps) of our PET/MR system, the detected differences were small in terms of regional bias. Statistically significant differences were seen only with two MRAC methods out of three when comparing the average error. Whereas no significant improvement was seen in correlation of MRAC reconstruction to CTAC reconstruction when applying TOF, although both correlation and fitting coefficients improved with TOF. Although, it would seem the use of TOF implies a smaller bias on average (Figure 6). However, we found implications that some regions might increase in bias compared to non-TOF reconstruction, similarly to Emond et al. [16], although TOF shows reduced variation on a global scale

(Figure 7). This effect was smaller when the accuracy of the attenuation map increased, making accurate attenuation correction a necessary prerequisite in neuroimaging, also when applying TOF, as recommended by Emond et al. [16].

As the Ingenuity TF PET/MR is capable of 525 ps timing resolution, more gain in quantitative accuracy could be achieved with a PET/MR system capable of higher timing resolution as suggested in [7]. Recently, several brain-dedicated PET imaging systems have been introduced with a timing resolution even close to 100 ps [27,28]. Thus, it would be worthwhile to investigate our preliminary findings on how much the accuracy of the PET images is affected by the accuracy of the attenuation maps used in these systems in combination of TOF, in addition to studying the changes in regional variation in accordance with TOF timing resolution. Thus, more gain in quantitative and visual accuracy in PET could be achieved when applying TOF with systems capable of higher timing resolutions and we strongly encourage further investigations on this matter.

Limitations

Due to the issues described in the paper of Maus et al. [29] concerning calibration of TOF and non-TOF reconstructions on the Ingenuity TF PET/MR, it was not possible to compare TOF and non-TOF reconstructions directly. In addition, comparing TOF and non-TOF reconstruction quantitatively is challenging due to the different convergence rates between TOF and non-TOF algorithms.

Moreover, using the Philips Ingenuity TF PET/MR system implies additional challenges in matching the reconstruction parameters between TOF and non-TOF reconstruction. As the system applies blob reconstruction, these parameters should be carefully selected to preserve visual quality and quantification. Since the reconstruction parameters are fixed for the algorithms, it is not possible to match them entirely for a more direct comparison.

For these reasons, all quantitative comparisons were performed in comparison of TOF MRAC vs. TOF CTAC and similarly in the non-TOF case throughout this paper. As this allows only a relative comparison of improvement, we suggest that future studies try to address this by direct comparison of the algorithms. We also encourage new investigations on this matter, with both recent whole-body and dedicated brain systems using a higher timing resolution than the system used in this study.

5. Conclusions

Using TOF reconstruction could be beneficial in reducing the quantitative errors due to imperfections in MRAC also in the head region and needs further investigation and validation with PET systems capable of higher timing resolution. Nevertheless, even when using TOF reconstruction, accurate attenuation correction remains a necessary prerequisite in PET/MR neuroimaging.

We have detected an effect where the majority of the regions showed reduced bias when TOF was applied; however, more bias, although small, was introduced in certain regions, confirming that the effect seen is indeed non-local. Overall, the differences seen in our study were small quantitatively and the improvements in average error were statistically significant only in two out of three MRAC methods when applying TOF. Although TOF reconstructions showed improvement in correlation and regression parameters, these differences were non-significant between TOF and non-TOF reconstructions.

As a continuation of our preliminary study, we strongly encourage further investigations on this matter to determine how large gains in quantitative and visual accuracy in PET could be achieved with TOF with systems capable of higher timing resolutions.

Author Contributions: Conceptualization, J.L. and J.T.; Data Curation, J.T.; Formal Analysis, J.L. and J.T.; Funding Acquisition, R.K. and M.T.; Investigation, J.L. and J.T.; Methodology, J.L. and J.T.; Project Administration, R.K. and M.T.; Software, J.T.; Supervision, R.K.; Validation, J.L.; Visualization, J.L. and J.T.; Writing—Original Draft, J.L. and J.T.; Writing—Review and Editing, J.L., J.T., R.K. and M.T. All authors have read and agreed to the published version of the manuscript.

Funding: This study was financially supported by The Finnish Cultural Foundation Grant ID 00150543, Grant from Division of Imaging TUCH, the Alfred Kordelin Foundation, The Paulo Foundation (Paulon Säätiö) and the Finnish Cultural Foundation, Varsinais-Suomi Regional Fund. Financial support was also received from State Research Funding (the expert responsibility area of TYKS, Turku University Hospital) (project numbers 13236, 13720), and grants from State funding for university-level health research, Turku University Hospital (11232).

Institutional Review Board Statement: The study was conducted as a retrospective registry study at Turku PET Centre (study number: T7/2021). The study protocol was approved by Turku University Hospital Research Board and the legislative team. The requirements for ethical review in Finland are stipulated primarily in the Medical Research Act (488/1999, as amended) and the Act of the Medical Use of Human Organs, Tissues and Cells (101/2001 as amended). Ethical review is statutorily required for interventional medical research and some circumstances for studies on human organs, tissues, or cells. According to Finnish legislation, no ethical assessment or approval by an independent review board is mandatory for registry studies. The study was conducted in accordance with the Declaration of Helsinki.

Informed Consent Statement: The need to acquire an active informed consent from the individuals included in the study was waived as the study was conducted as a retrospective registry study at Turku PET Centre.

Data Availability Statement: Although all data cannot be shared because of patient confidentiality, some data generated or used during the study are available from the corresponding author by request. The source codes for the methods presented in this paper can be downloaded free of charge from the GitLab account (https://gitlab.utu.fi/jjlind, accessed on 19 April 2022) of the corresponding author, hosted by the University of Turku, or by contacting the corresponding author directly (J. Lindén).

Acknowledgments: We want to acknowledge Jouni Tuisku for the assistance in implementing the data analysis pipeline and Hidehiro Iida for helpful discussion and ideas in implementing this study. The authors thank Philips Healthcare for providing tools for using an off-line attenuation map for PET reconstruction and technical assistance for implementing the TOF reconstruction protocol for brain image reconstruction.

Conflicts of Interest: The authors declare no conflict of interest. The funders had no role in the design of the study; in the collection, analyses, or interpretation of data; in the writing of the manuscript; or in the decision to publish the results.

Appendix A. VOI Analysis Result Tables

Table A1. The mean of the bias across the brain regions with all attenuation maps with TOF and non-TOF reconstructions. The color of the DIFF column indicates the direction of the change. Green comparisons improve, and red comparisons get larger error.

	2-Class MRAC (No Air)			2-Class MRAC			3-Class MRAC		
	Non-TOF	**TOF**	**DIFF**	**Non-TOF**	**TOF**	**DIFF**	**Non-TOF**	**TOF**	**DIFF**
Precentral	−6.55%	−6.43%	−0.12%	−6.67%	−6.58%	−0.09%	−2.86%	−3.02%	0.16%
Rolandic_Oper	−3.99%	−3.45%	−0.54%	−4.18%	−3.75%	−0.43%	−2.33%	−2.49%	0.16%
Supp_Motor Area	−4.92%	−5.66%	0.74%	−5.04%	−5.79%	0.75%	−3.34%	−3.10%	−0.24%
Olfactory	−4.20%	−4.77%	0.57%	−4.64%	−5.16%	0.52%	−2.77%	−2.84%	0.07%
Region #5	−5.40%	−5.80%	0.40%	−5.88%	−6.23%	0.35%	−2.94%	−2.99%	0.05%
Frontal_Sup	−6.39%	−6.38%	−0.02%	−6.83%	−6.70%	−0.13%	−3.39%	−3.19%	−0.20%
Frontal_Mied	−6.37%	−5.54%	−0.83%	−6.94%	−6.05%	−0.90%	−2.84%	−2.79%	−0.05%
Frontal_Inf	−4.85%	−3.54%	−1.31%	−5.25%	−4.12%	−1.13%	−1.82%	−2.08%	0.26%
Rectus	0.01%	−1.59%	1.61%	−1.26%	−2.21%	0.94%	−1.44%	−2.30%	0.86%
Insula	−0.80%	−0.94%	0.14%	−1.11%	−1.30%	0.19%	−2.50%	−2.22%	−0.28%
Cingulum_Ant	−1.08%	−2.03%	0.95%	−1.25%	−2.21%	0.96%	−2.88%	−2.25%	−0.62%
Cingulum_Mid	−1.14%	−2.54%	1.40%	−1.28%	−2.71%	1.43%	−3.02%	−2.62%	−0.40%
Cingulum_Post	−2.78%	−3.23%	0.45%	−3.11%	−3.82%	0.71%	−3.29%	−2.83%	−0.45%
Hippocampus/ ParaHippocampal	−0.78%	−1.22%	0.43%	−1.29%	−2.15%	0.86%	−3.59%	−2.94%	−0.66%
Amygdala	−3.38%	−3.38%	0.01%	−3.83%	−4.23%	0.40%	−3.74%	−3.06%	−0.68%

Table A1. *Cont.*

	2-Class MRAC (No Air)			2-Class MRAC			3-Class MRAC		
	Non-TOF	**TOF**	**DIFF**	**Non-TOF**	**TOF**	**DIFF**	**Non-TOF**	**TOF**	**DIFF**
Calcarine	−4.24%	−3.17%	−1.07%	−4.53%	−3.75%	−0.78%	−3.74%	−2.67%	−1.07%
Cuneus	−6.67%	−5.38%	−1.28%	−6.86%	−5.82%	−1.04%	−4.20%	−3.30%	−0.89%
Lingual	−4.03%	−3.22%	−0.80%	−4.50%	−4.18%	−0.32%	−3.61%	−2.67%	−0.94%
Occipital	−10.67%	−9.17%	−1.51%	−10.85%	−9.72%	−1.13%	−3.97%	−3.66%	−0.32%
Fusiform	−5.43%	−3.25%	−2.18%	−6.70%	−5.28%	−1.42%	−4.77%	−3.32%	−1.45%
Postcentral	−6.79%	−6.20%	−0.59%	−6.99%	−6.53%	−0.46%	−2.83%	−2.87%	0.04%
SupraMarginal	−5.57%	−4.71%	−0.86%	−6.23%	−5.72%	−0.51%	−3.28%	−2.81%	−0.47%
Angular	−6.63%	−5.98%	−0.65%	−6.93%	−6.45%	−0.47%	−2.32%	−2.47%	0.15%
Precuneus	−8.52%	−7.73%	−0.79%	−8.77%	−8.15%	−0.62%	−3.14%	−2.91%	−0.23%
Paracentral Lobule	−5.20%	−4.70%	−0.51%	−5.42%	−4.98%	−0.44%	−3.70%	−3.01%	−0.69%
Caudate	−5.72%	−5.28%	−0.43%	−6.18%	−6.01%	−0.17%	−3.51%	−2.92%	−0.60%
Putamen	−0.71%	−1.51%	0.81%	−1.18%	−2.21%	1.03%	−2.56%	−2.07%	−0.48%
Pallidum	−2.40%	−2.49%	0.10%	−3.00%	−3.28%	0.28%	−2.88%	−2.55%	−0.33%
Thalamus	−6.47%	−5.15%	−1.32%	−7.41%	−6.62%	−0.79%	−3.69%	−3.15%	−0.55%
Heschl	−4.18%	−3.78%	−0.40%	−4.86%	−4.84%	−0.02%	−3.28%	−2.75%	−0.53%
Parietal	−6.16%	−4.96%	−1.21%	−6.98%	−6.17%	−0.80%	−3.43%	−3.00%	−0.42%
Temporal	−8.32%	−8.02%	−0.29%	−8.60%	−8.40%	−0.19%	−3.20%	−3.33%	0.13%
Vermis	−7.29%	−4.29%	−3.00%	−7.80%	−5.77%	−2.04%	−2.99%	−2.12%	−0.87%
Cerebellum Crus	−5.85%	−4.51%	−1.35%	−7.98%	−7.88%	−0.10%	−4.93%	−4.34%	−0.59%
Cerebellum	−6.62%	−5.14%	−1.47%	−9.63%	−9.38%	−0.25%	−5.25%	−4.80%	−0.45%

Table A2. The standard deviation of the bias across the brain regions with all attenuation maps with TOF and non-TOF reconstructions.

	2-Class MRAC (No Air)		2-Class MRAC		3-Class MRAC	
	Non-TOF	**TOF**	**Non-TOF**	**TOF**	**Non-TOF**	**TOF**
Precentral	2.10%	2.38%	2.15%	2.41%	1.65%	1.83%
Rolandic_Oper	1.99%	2.02%	2.01%	2.00%	1.69%	1.76%
Supp_Motor Area	2.02%	2.36%	2.03%	2.38%	1.60%	1.91%
Olfactory	1.67%	1.93%	1.83%	2.02%	1.60%	1.77%
Region #5	1.90%	2.20%	2.05%	2.29%	1.72%	1.85%
Frontal_Sup	2.16%	2.23%	2.17%	2.26%	1.66%	1.65%
Frontal_Mied	2.19%	2.21%	2.24%	2.18%	1.76%	1.70%
Frontal_Inf	2.21%	2.19%	2.32%	2.19%	1.91%	1.80%
Rectus	1.95%	1.92%	2.41%	2.02%	2.44%	1.97%
Insula	1.62%	1.86%	1.61%	1.80%	1.53%	1.74%
Cingulum_Ant	1.57%	1.86%	1.46%	1.83%	1.24%	1.62%
Cingulum_Mid	1.57%	2.14%	1.51%	2.13%	1.32%	1.81%
Cingulum_Post	1.56%	2.06%	1.55%	2.04%	1.40%	1.88%
Hippocampus/ ParaHippocampal	1.78%	1.96%	1.86%	2.22%	1.62%	2.08%
Amygdala	1.90%	2.15%	2.02%	2.27%	1.80%	2.08%
Calcarine	1.67%	1.91%	1.67%	1.78%	1.55%	1.76%

Table A2. *Cont.*

	2-Class MRAC (No Air)		2-Class MRAC		3-Class MRAC	
	Non-TOF	**TOF**	**Non-TOF**	**TOF**	**Non-TOF**	**TOF**
Cuneus	1.73%	2.03%	1.73%	1.93%	1.64%	1.83%
Lingual	1.51%	1.82%	1.48%	1.67%	1.55%	1.85%
Occipital	2.30%	2.18%	2.33%	2.07%	2.14%	2.11%
Fusiform	1.64%	2.15%	1.70%	1.91%	1.54%	1.87%
Postcentral	2.15%	2.30%	2.14%	2.27%	1.88%	1.94%
SupraMarginal	1.77%	2.10%	1.68%	1.92%	1.62%	1.94%
Angular	2.33%	2.53%	2.26%	2.42%	1.89%	2.06%
Precuneus	2.42%	2.80%	2.37%	2.70%	2.02%	2.29%
Paracentral Lobule	1.53%	2.24%	1.50%	2.18%	1.42%	1.84%
Caudate	2.01%	2.48%	1.95%	2.39%	1.74%	2.12%
Putamen	1.40%	1.86%	1.29%	1.72%	1.25%	1.75%
Pallidum	1.49%	1.81%	1.52%	1.70%	1.62%	1.83%
Thalamus	1.79%	2.10%	1.88%	2.00%	1.86%	2.05%
Heschl	1.66%	2.09%	1.62%	1.95%	1.55%	1.90%
Parietal	1.75%	2.06%	1.71%	1.93%	1.73%	1.94%
Temporal	2.23%	2.66%	2.19%	2.62%	2.01%	2.13%
Vermis	2.18%	2.29%	2.28%	2.44%	2.08%	2.33%
Cerebellum Crus	2.19%	2.37%	2.31%	2.21%	1.97%	2.10%
Cerebellum	2.35%	2.55%	2.56%	2.54%	2.12%	2.32%

References

1. Zaidi, H.; Ojha, N.; Morich, M.; Griesmer, J.; Hu, Z.; Maniawski, P.; Ratib, O.; Izquierdo-Garcia, D.; Fayad, Z.A.; Shao, L. Design and performance evaluation of a whole-body Ingenuity TF PET–MRI system. *Phys. Med. Biol.* **2011**, *56*, 3091. [CrossRef]
2. Grant, A.M.; Deller, T.W.; Khalighi, M.M.; Maramraju, S.H.; Delso, G.; Levin, C.S. NEMA NU 2-2012 performance studies for the SiPM-based ToF-PET component of the GE SIGNA PET/MR system. *Med. Phys.* **2016**, *43*, 2334–2343. [CrossRef]
3. Chen, S.; Gu, Y.; Yu, H.; Chen, X.; Cao, T.; Hu, L.; Shi, H. NEMA NU2-2012 performance measurements of the United Imaging uPMR790: An integrated PET/MR system. *Eur. J. Nucl. Med. Mol. Imaging* **2021**, *48*, 1726–1735. [CrossRef]
4. Van Sluis, J.; De Jong, J.; Schaar, J.; Noordzij, W.; Van Snick, P.; Dierckx, R.; Borra, R.; Willemsen, A.; Boellaard, R. Performance Characteristics of the Digital Biograph Vision PET/CT System. *J. Nucl. Med.* **2019**, *60*, 1031–1036. [CrossRef]
5. Conti, M. State of the art and challenges of time-of-flight PET. *Phys. Med. Eur. J. Med. Phys.* **2009**, *25*, 1–11. [CrossRef]
6. Conti, M. Why is TOF PET reconstruction a more robust method in the presence of inconsistent data? *Phys. Med. Biol.* **2011**, *56*, 155–168. [CrossRef]
7. Mehranian, A.; Zaidi, H. Impact of time-of-flight PET on quantification errors in MR imaging-based attenuation correction. *J. Nucl. Med.* **2015**, *56*, 635–641. [CrossRef]
8. Conti, M.; Bendriem, B. The new opportunities for high time resolution clinical TOF PET. *Clin. Transl. Imaging* **2019**, *7*, 139–147. [CrossRef]
9. Mehranian, A.; Arabi, H.; Zaidi, H. Vision 20/20: Magnetic resonance imaging-guided attenuation correction in PET/MRI: Challenges, solutions, and opportunities. *Med. Phys.* **2016**, *43*, 1130–1155. [CrossRef]
10. Davison, H.; Ter Voert, E.E.G.W.; De Galiza Barbosa, F.; Veit-Haibach, P.; Delso, G. Incorporation of Time-of-Flight Information Reduces Metal Artifacts in Simultaneous Positron Emission Tomography/Magnetic Resonance Imaging: A Simulation Study. *Investig. Radiol.* **2015**, *50*, 423–429. [CrossRef]
11. Svirydenka, H.; Delso, G.; De Galiza Barbosa, F.; Huellner, M.; Davison, H.; Fanti, S.; Veit-Haibach, P.; Ter Voert, E.E.G.W. The Effect of Susceptibility Artifacts Related to Metallic Implants on Adjacent-Lesion Assessment in Simultaneous TOF PET/MR. *J. Nucl. Med.* **2017**, *58*, 1167–1173. [CrossRef]
12. Ter Voert, E.E.G.W.; Delso, G.; de Galiza Barbosa, F.; Huellner, M.; Veit-Haibach, P. The Effect of Defective PET Detectors in Clinical Simultaneous [^{18}F]FDG Time-of-Flight PET/MR Imaging. *Mol. Imaging Biol.* **2017**, *19*, 626–635. [CrossRef]
13. Delso, G.; Khalighi, M.; ter Voert, E.; Barbosa, F.; Sekine, T.; Hüllner, M.; Veit-Haibach, P. Effect of Time-of-Flight Information on PET/MR Reconstruction Artifacts: Comparison of Free-breathing versus Breath-hold MR-based Attenuation Correction. *Radiology* **2017**, *282*, 229–235. [CrossRef]

14. Ter Voert, E.E.G.W.; Veit-Haibach, P.; Ahn, S.; Wiesinger, F.; Khalighi, M.M.; Levin, C.S.; Iagaru, A.H.; Zaharchuk, G.; Huellner, M.; Delso, G. Clinical evaluation of TOF versus non-TOF on PET artifacts in simultaneous PET/MR: A dual centre experience. *Eur. J. Nucl. Med. Mol. Imaging* **2017**, *44*, 1223–1233. [CrossRef]
15. Boellaard, R.; Hofman, M.B.M.; Hoekstra, O.S.; Lammertsma, A.A. Accurate PET/MR quantification using time of flight MLAA image reconstruction. *Mol. Imaging Biol.* **2014**, *16*, 469–477. [CrossRef]
16. Emond, E.C.; Bousse, A.; Machado, M.; Porter, J.; Groves, A.M.; Hutton, B.F.; Thielemans, K. Effect of attenuation mismatches in time of flight PET reconstruction. *Phys. Med. Biol.* **2020**, *65*, 085009. [CrossRef]
17. Teuho, J.; Torrado-Carvajal, A.; Herzog, H.; Anazodo, U.; Klén, R.; Iida, H.; Teräs, M. Magnetic Resonance-Based Attenuation Correction and Scatter Correction in Neurological Positron Emission Tomography/Magnetic Resonance Imaging—Current Status With Emerging Applications. *Front. Phys.* **2020**, *7*, 243. [CrossRef]
18. Ladefoged, C.N.; Law, I.; Anazodo, U.; Lawrence, K.S.; Izquierdo-Garcia, D.; Catana, C.; Burgos, N.; Cardoso, M.J.; Ourselin, S.; Hutton, B.; et al. A multi-centre evaluation of eleven clinically feasible brain PET/MRI attenuation correction techniques using a large cohort of patients. *Neuroimage* **2017**, *147*, 346–359. [CrossRef]
19. Bettinardi, V.; Presotto, L.; Rapisarda, E.; Picchio, M.; Gianolli, L.; Gilardi, M.C. Physical performance of the new hybrid PET/CT Discovery-690. *Med. Phys.* **2011**, *38*, 5394–5411. [CrossRef]
20. Burger, C.; Goerres, G.; Schoenes, S.; Buck, A.; Lonn, A.; Von Schulthess, G. PET attenuation coefficients from CT images: Experimental evaluation of the transformation of CT into PET 511-keV attenuation coefficients. *Eur. J. Nucl. Med.* **2002**, *29*, 922–927. [CrossRef]
21. Schramm, G.; Langner, J.; Hofheinz, F.; Petr, J.; Beuthien-Baumann, B.; Platzek, I.; Steinbach, J.; Kotzerke, J.; Van Den Hoff, J. Quantitative accuracy of attenuation correction in the Philips Ingenuity TF whole-body PET/MR system: A direct comparison with transmission-based attenuation correction. *Magma* **2013**, *26*, 115–126. [CrossRef]
22. Teuho, J.; Linden, J.; Johansson, J.; Tuisku, J.; Tuokkola, T.; Teräs, M. Tissue Probability-Based Attenuation Correction for Brain PET/MR by Using SPM8. *IEEE Trans. Nucl. Sci.* **2016**, *63*, 2452–2463. [CrossRef]
23. Wald, A. Asymptotically Shortest Confidence Intervals. *Ann. Math. Stat.* **1942**, *13*, 127–137. [CrossRef]
24. Benjamini, Y.; Hochberg, Y. Controlling the False Discovery Rate: A Practical and Powerful Approach to Multiple Testing. *J. R. Stat. Soc. Ser. B* **1995**, *57*, 289–300. [CrossRef]
25. Ouyang, J.; Chun, S.Y.; Petibon, Y.; Bonab, A.A.; Alpert, N.; El Fakhri, G. Bias atlases for segmentation-based pet attenuation correction using PET-CT and MR. *IEEE Trans. Nucl. Sci.* **2013**, *60*, 3373–3382. [CrossRef]
26. Khalifé, M.; Fernandez, B.; Jaubert, O.; Soussan, M.; Brulon, V.; Buvat, I.; Comtat, C. Subject-specific bone attenuation correction for brain PET/MR: Can ZTE-MRI substitute CT scan accurately? *Phys. Med. Biol.* **2017**, *62*, 7814–7832. [CrossRef]
27. Lee, M.S.; Cates, J.W.; Gonzalez-Montoro, A.; Levin, C.S. High-resolution time-of-flight PET detector with 100 ps coincidence time resolution using a side-coupled phoswich configuration. *Phys. Med. Biol.* **2021**, *66*, 125007. [CrossRef]
28. Schaart, D.R.; Schramm, G.; Nuyts, J.; Surti, S. Time of Flight in Perspective: Instrumental and Computational Aspects of Time Resolution in Positron Emission Tomography. *IEEE Trans. Radiat. Plasma Med. Sci.* **2021**, *5*, 598. [CrossRef]
29. Maus, J.; Schramm, G.; Hofheinz, F.; Oehme, L.; Lougovski, A.; Petr, J.; Platzek, I.; Beuthien-Baumann, B.; Steinbach, J.; Kotzerke, J.; et al. Evaluation of in vivo quantification accuracy of the Ingenuity-TF PET/MR. *Med. Phys.* **2015**, *42*, 5773–5781. [CrossRef]